Applied Catalysis B: Environmental 99 (2010) 89–95

Contents lists available at ScienceDirect

Applied Catalysis B: Environmental

journal homepage: www.elsevier.com/locate/apcatb

Au-mixed lanthanum/cerium oxide catalysts for water gas shift

Yanan Wang[a,b], Shuang Liang[a,b], Anmin Cao[a,b], Robert L. Thompson[a,c], Götz Veser[a,b,*]

[a] US DOE-National Energy Technology Laboratory, Pittsburgh, PA 15263, United States
[b] Chemical Engineering Department, Swanson School of Engineering, University of Pittsburgh, Pittsburgh, PA 15261, United States
[c] Parsons, South Park, PA 15129, United States

ARTICLE INFO

Article history:
Received 7 December 2009
Received in revised form 16 April 2010
Accepted 3 June 2010
Available online 11 June 2010

Keywords:
Water gas shift
Gold
Mixed La/Ce-oxide
Activity
Reducibility

ABSTRACT

We report on the synthesis of highly homogeneous mixed La/Ce-oxides via a microemulsion-templated approach, and their evaluation as active supports for Au in the water gas shift (WGS) reaction. Both structure and reducibility of the oxides could be tailored by adjusting the La content across the entire range of La:Ce-ratios. The reducibility of the Au-free oxides shows an optimum at ~25% La content, which can be traced back to improved oxygen mobility due to formation of oxygen vacancies and to the formation of more strongly bound oxygen upon La addition.

Deposition of Au onto these oxides gives rise to an additional, low-temperature reduction peak, presumably due to hydrogen spill-over from the noble metal onto the oxide support. The WGS activity of $Au/La_xCe_{1-x}O_{2-0.5x}$ catalysts correlates closely with the reducibility of the oxide supports, and hence with La content, demonstrating that carefully controlled synthesis of nanostructured catalysts with uniform, tailored composition allows for fine control of reactive properties of these materials, and might ultimately open the way towards a more rational design of catalysts.

1. Introduction

The water gas shift reaction (WGS) plays a critical role in the production of hydrogen from fossil and renewable resources. It has attracted great attention because of its applications in producing syngas for chemicals and liquid fuels, providing hydrogen-rich streams for fuel cells [1,2] and processing exhaust gases from automobiles [3–6]. WGS is an exothermal reaction and thus limited by thermodynamic equilibrium at high temperatures. At low temperatures, the thermodynamics are favorable, but the reaction is constrained by slow kinetics. Current industrial WGS processes therefore utilize a two-stage process involving a high-temperature shift catalyst (typically Fe–Cr-based) and a low-temperature shift catalyst ($Cu/ZnO/Al_2O_3$) in order to take advantage of fast reaction kinetics at high-temperature and high-equilibrium conversion at low temperature. However, these catalysts are not suitable for portable applications because of insufficient stability and activity. Hence, much effort is currently focused on the development of more active and durable catalysts for WGS.

Gold supported on metal oxides has been widely used in CO oxidation and, more recently, in WGS. Since the nature of the catalyst support exerts a decisive influence on the catalytic activity [7,8], the impact of metal oxide supports has been investigated extensively in WGS [9,10]. Among those, CeO_2 is one of the most effective (and active) supports for Au catalysts, although the role played by CeO_2 is still a matter of debate [11]. Previous studies showed that the active species in Au/CeO_2 catalysts are isolated $Au^{\delta+}$ cations [12], and that redox properties and oxygen storage capacity of CeO_2 are crucial for the activity of the Au/CeO_2 catalysts [12–14]. In particular, it has been reported that the addition of rare earth additives affects redox properties and oxygen vacancies in ceria [15,16], which can strongly impact catalyst activity [17–19]. However, there is still significant disagreement in the literature and very few systematic studies of such doped-CeO_2 catalysts for WGS are available due to difficulties in synthesizing well-controlled homogeneous mixed oxides, especially in the high doping range.

The main target of the present study was therefore to develop a better understanding of the function of rare earth additives in Au/ceria WGS catalysis based on mixed ceria/lanthana as example system. Mixed La/Ce-oxides were synthesized over a broad range of La content (10–75%) via a carefully controlled reverse microemulsion-templated sol–gel synthesis route [20]. Highly homogeneous mixed La/Ce-oxide solid solutions were obtained over the entire range of La-dopings without phase separation. After deposition of Au onto these mixed oxides by deposition–precipitation, a clear correlation of the catalyst activity with the reducibility of the mixed oxide support was obtained.

* Corresponding author at: 1249 Benedum Hall, University of Pittsburgh, Pittsburgh, PA 15261, United States. Tel.: +1 412 624 1042; fax: +1 412 624 9639.
E-mail address: gveser@pitt.edu (G. Veser).

0926-3373/$ – see front matter © 2010 Elsevier B.V. All rights reserved.
doi:10.1016/j.apcatb.2010.06.004

2. Experimental

2.1. Catalyst preparation and characterization

Pure and mixed La/Ce-oxides ($La_xCe_{1-x}O_{2-0.5x}$) with different La contents were synthesized through hydrolysis of cerium and lanthanum isopropoxide in a reverse (water-in-oil) microemulsion. The microemulsion was composed of water, isooctane (2,2,4-trimethylpentane, 99.7% Aldrich), poly(ethylene oxide)-block-poly(propylene oxide)-block-poly(ethylene oxide) with 10 wt% ethylene oxide (Aldrich) and 1-pentanol (99+%, Aldrich) as a co-surfactant. The metal isopropoxide precursor solution (Ce- and La-isopropoxide in isopropanol) was added to the microemulsion at the desired La:Ce-ratio, and the solution was aged for 70 h under constant stirring at room temperature. After phase separation, the gel was washed in acetone four times, freeze-dried, and finally calcined at 450 °C for 4 h.

$Au/La_xCe_{1-x}O_{2-0.5x}$ samples were prepared by deposition–precipitation (DP) [11]. $HAuCl_4$ (99.9+%, Aldrich) solution was added drop-wise at room temperature into an aqueous slurry of the oxide, keeping the pH of slurry fixed via addition of 0.2 M $(NH_4)_2CO_3$ (93.5+%, J.T. Baker). The resulting precipitate was aged at room temperature for 1 h, filtered, washed, dried at 100 °C, and then calcined at 400 °C for 2 h. The nominal Au loading for all catalysts was 5 wt%.

The actual Au content of each sample was analyzed by inductively coupled plasma mass spectrometry (ICP-MS, Perkin Elmer Elan DRC II). BET surface area and pore distribution of the materials were determined via nitrogen sorption using the BET method (Micromeritics ASAP 2010 gas adsorption analyzer). X-ray diffraction (Phillips PW1830) measurement was used to identify crystal structures. The diffraction patterns were recorded in the range of 10–80° with a step of 0.02°(2θ). The particle size of the oxides estimated from this data via standard Debye–Scherrer analysis.

Transmission electron microscopy was performed on JEOL-2000FX and JEOL JEM-2100F electron microscopes. Samples were dispersed on a copper type-B support grid (Ted Pella Inc.).

Temperature-programmed reduction by hydrogen (H_2-TPR) was conducted using a Micromeritics Chemisorb 2750 chemisorption system equipped with a thermal conductivity detector. Sample in powder form was first oxidized in air for 30 min with a subsequent flush with He for 30 min, both at 400 °C, and then cooled down to room temperature. The sample was then heated at a rate of 5 °C/min from room temperature to 900 °C in 10% H_2/Ar. A cooling trap filled with acetone–dry ice mixture located between the reactor and TCD was used to trap the water generated by the reaction. The exit gas during the whole procedure was monitored using mass spectrometry (Balzers Quadstar GSD 300) for time resolved, quantitative measurement of gas composition.

2.2. Catalyst tests

Water gas shift tests were carried out in a 5 mm ID quartz glass tube heated inserted into a high-temperature tube furnace at ambient pressure. The catalyst powder (50 mg) was supported within the tube on either end by quartz glass felt plugs. Water was injected via a syringe pump (Braintree Scientific, Inc.) and vaporized in a heated line before entering the reactor. The composition of the mixture after water addition was 10.78% H_2O, 2.08% CO, and 87.14% He. The total flow rate of gas was typically around 100 CCM resulting in space velocities of ~150,000 h^{-1}. The exit gas passed through a condenser to eliminate H_2O from the stream and then was analyzed by an Agilent 3000A Micro GC equipped with thermal conductivity detector (TCD). In order to assure reaching steady state after adjusting operating conditions (such as temperature steps), CO conversion was measured repeatedly until the conversion varied less than 1% over a duration 5 min. No methane was detected at any conditions used in this work. The inert helium feed is used as an internal standard, and is used to calculate the total gas flow rate after water condensation and to back-calculate the concentration of water leaving the reactor.

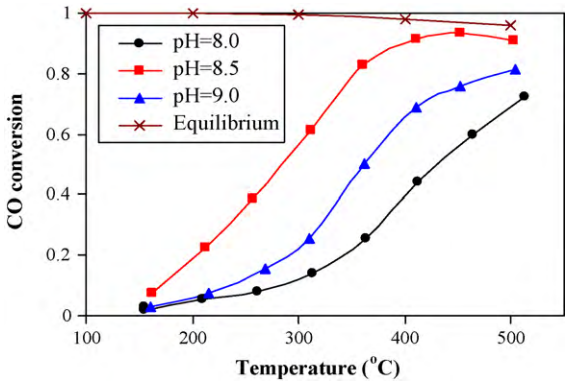

Fig. 1. Catalytic activity of $Au/La_{0.5}Ce_{0.5}O_{1.75}$ catalysts prepared at different pH during deposition–precipitation. CO conversion is shown as a function of reaction temperature.

3. Results and discussion

3.1. Effect of pH value upon Au deposition

The pH value is an important factor in the preparation of supported Au catalysts by deposition–precipitation (DP), because it can significantly affect the Au loading and particle size, resulting in corresponding differences in catalytic activity [21]. Therefore, the effect of the pH value on Au deposition via DP on mixed La/Ce-oxides was first studied before investigating the influence of La doping on the catalyst activity. In order to establish optimum pH values for the mixed oxides as a function of La content, all oxides were synthesized at different pH values. Here, the properties of $Au/La_{0.5}Ce_{0.5}O_{1.75}$ catalysts prepared at pH values of 8, 8.5 and 9 are discussed in detail to illustrate the general findings.

Fig. 1 shows the activities of $Au/La_{0.5}Ce_{0.5}O_{1.75}$ catalysts obtained at different pH values in terms of CO conversion as function of temperature. The WGS activity of the catalysts increases as the pH increases from 8.0 to 8.5, and then decreases again for the sample synthesized at pH = 9.0. In order to explain this optimal pH value, the samples were characterized via XRD and ICP-MS in order to evaluate Au loading and particle size. (It should be noted that it was not possible to evaluate Au particle size via TEM since Au does not give enough contrast against the Ce/La-oxides for reliable differentiation. Also, measurement of Au dispersion via CO or H_2 chemisorption, reported before for low ceria-content Au/ceria-titania samples [22], did not result in robust and reliable data in our case, possibly due to the much higher ceria content. Furthermore, no suitable probe molecule is known which adsorbs selectively on Au but not on the oxide supports.)

The XRD patterns of the three synthesized $Au/La_{0.5}Ce_{0.5}O_{1.75}$ catalysts are shown in Fig. 2. The diffraction patterns are strongly dominated by reflections due to the oxide. However, a Au diffraction peak appears (at $2\theta = 39°$) when Au was precipitated at pH 8.0, indicating the appearance of larger Au particles. Samples obtained at higher pH value do not show this reflection, suggesting that the Au particles at higher pH values are below the XRD detection limit. This difference in Au particle size may be caused by the chloride in the precursor. At pH above 8.5, anionic Au complexes are the major species in the solution and most of the chloride, which has been shown to cause aggregation of Au particles [21], has been removed

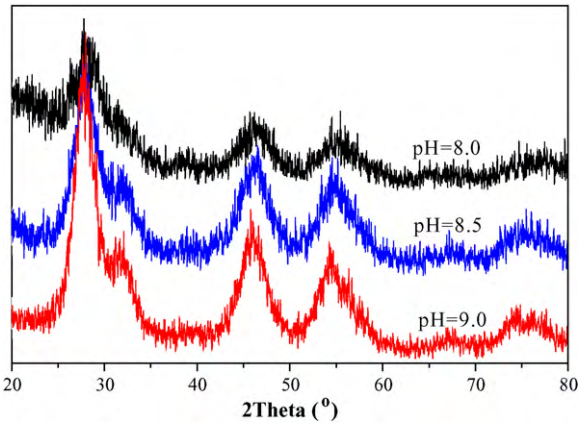

Fig. 2. XRD patterns of $Au/La_{0.5}Ce_{0.5}O_{1.75}$ obtained at different pH values.

Table 1
Physical properties of $Au/La_{0.5}Ce_{0.5}O_{1.75}$ catalysts precipitated at different pH values.

pH	Surface area (m^2/g)	Pore volume (cm^3/g)	Au (wt%)
8	50.9	0.13	4.69
8.5	82.1	0.14	3.15
9.0	95.0	0.18	1.16

by hydrolysis. Hence, after calcination, Au particles are small and uniform. In contrast, for pH below 8.5, residual chloride results in the growth of the Au particles during calcinations, leading to reduced Au surface area and hence reduced activity with decreasing pH during Au deposition. The formation of larger Au particles at lower pH also results in decreasing pore volume and total surface area (see Table 1), presumably by blocking some of the pores of the support.

In contrast to that, ICP-MS measurements show a decreasing Au content in the catalyst with the increasing of pH, as shown in Table 1. This can be explained by the increasingly negatively charged surface with increasing pH, resulting in an electrostatic repulsion of $AuCl_4^-$, and hence reduced yield during the deposition process.

Superposition of the two counter-acting effects – decreasing Au particle size and decreasing Au loading with increasing pH – results in an optimum catalyst activity at intermediate pH, as seen in Fig. 1.

This optimum pH, which results in the most active catalyst, is a function of the La:Ce-ratio in the mixed oxides. Fig. 3 shows the optimum pH vs. La content (as metal percent) based on detailed investigations of the pH effect on the activity of a range of Au on mixed La/Ce-oxides, similar to the discussion above for the La:Ce = 1:1 catalyst. One can see that the optimum pH value is initially constant at ~8.0 up to a La content of 25% (i.e. La:Ce = 1:3). Above 25% La, it increases with increasing La content, in agreement with the increasing IEP point of the mixed oxide. It has been previously reported that the optimal pH value for Au deposition corresponded to the IEP of the support [23]. However, CeO_2 and La_2O_3 have different isoelectric points (IEPs), with the former in the range of 5.2–8.6 [24] and the latter at 10.4 [25]. Hence, incorporation of La into the CeO_2 lattice can be expected to increase the IEP, and a higher pH is needed to neutralize the surface charges of $La_xCe_{1-x}O_{2-0.5x}$ with increasing La content in order to obtain small Au particles, as discussed above.

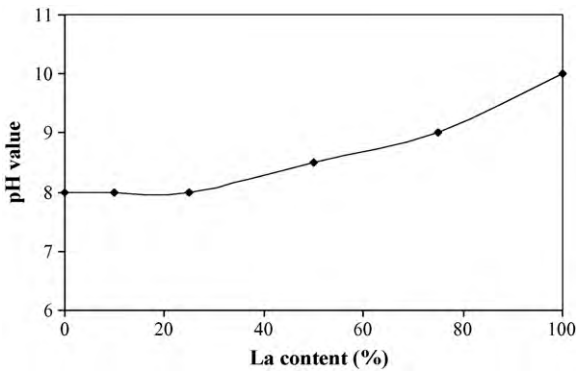

Fig. 3. Optimum pH values for depositing Au on $La_xCe_{1-x}O_{2-0.5x}$ as a function of La content.

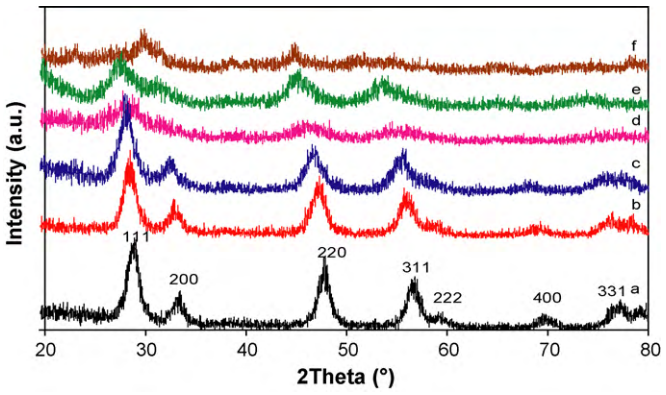

Fig. 4. XRD patterns of select $Au/La_xCe_{1-x}O_{2-0.5x}$ samples with varying La content (a: $x = 0$, b: $x = 0.10$, c: $x = 0.25$, d: $x = 0.5$, e: $x = 0.75$, f: $x = 1$).

Based on this evaluation of the pH on catalyst activity, all $Au/La_xCe_{1-x}O_{2-0.5x}$ samples used for further investigations into the effect of La doping were synthesized at their respective optimum pH values in order to exclude effects of Au loading or particle size.

3.2. Effect of La content on sample structure

In order to evaluate the effect of La content on the catalyst samples, the catalysts were first characterized via XRD (Fig. 4). The diffractograms for all samples show the six dominant reflections of the cubic fluorite-structure of ceria, corresponding to the (1 1 1), (2 0 0), (2 2 0), (3 1 1), (2 2 2), and (4 0 0) planes of the *fcc* structure. In agreement with our previous study of mixed La/Ce-oxides [26], no reflections characteristic of La_2O_3 were observed, even at a La content as high as 75%. Only the pure La_2O_3 sample shows the expected *hcp* reflections (Fig. 4, top curve "f"). This confirms the absence of any phase separation in these samples, i.e. the formation of a single, highly homogeneous mixed oxide phase.

Finally, no obvious Au peaks were detected, indicating that the Au particles are too small to be detected by XRD in all samples (<3 nm).

Fig. 5 shows the TEM images of pure CeO_2 (top left), Au/CeO_2 (top right), and two representative HR-TEM images of $Au/La_xCe_{1-x}O_{2-0.5x}$ mixed oxide catalysts (bottom left: $x = 0.25$; bottom right: $x = 0.5$). All samples consist of loosely agglomerated, roughly spherical nanoparticles. The addition of Au has no obvious effect on the morphology and the particle size of the supports. However, a slight decrease in particle size was found after La doping, from mean particle diameters of 7.6 nm for CeO_2 to 5.5 nm for $La_{0.5}Ce_{0.5}O_{1.75}$. This agrees qualitatively with previous results during Zr-doping of CeO_2 [27]. As mentioned before, the Au particles cannot be distinguished in the TEM micrographs since the oxides and Au nanoparticles have similar contrast.

For the $Au/La_xCe_{1-x}O_{2-0.5x}$ mixed oxide catalysts, very uniform lattice fringes are observed in the HR-TEM images, indicating high crystallinity of the samples. Analysis of the lattice fringes reveals a

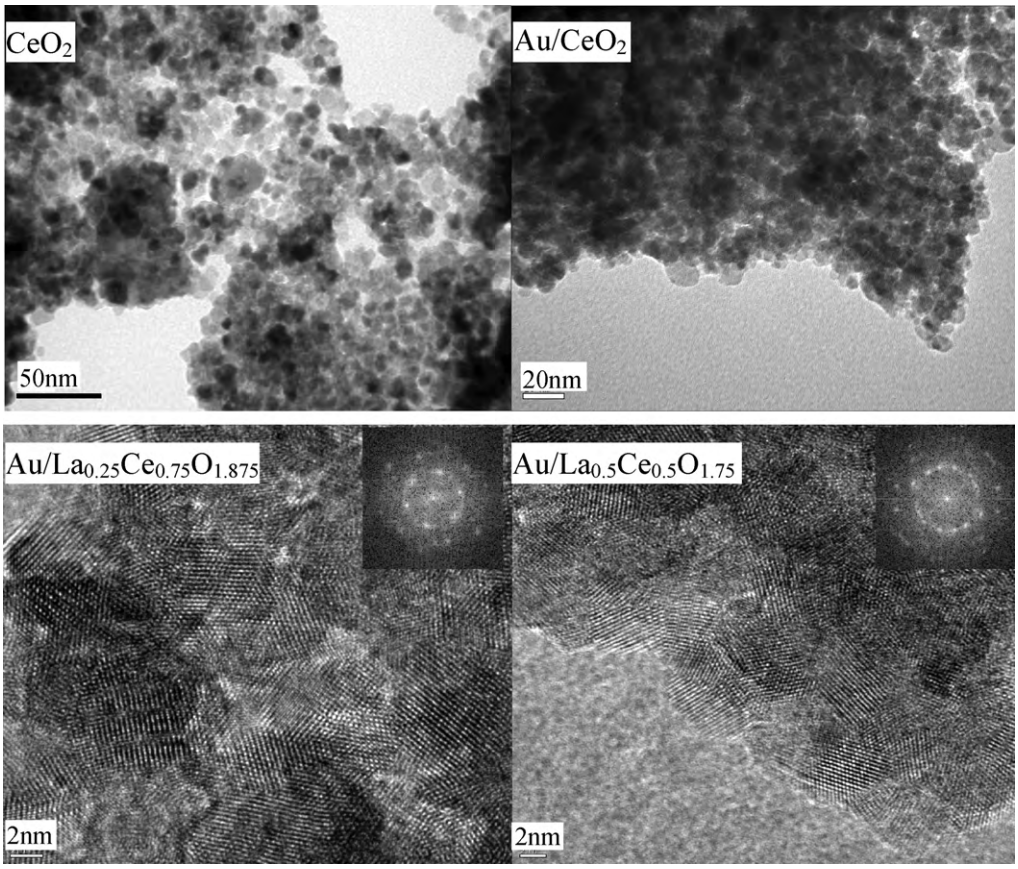

Fig. 5. TEM images of CeO_2, Au/CeO_2 (top row), and HR-TEM images of $Au/La_{0.25}Ce_{0.75}O_{1.875}$ and $Au/La_{0.5}Ce_{0.5}O_{1.75}$ (bottom row).

cubic structure with mainly (1 1 1) surface exposed, in agreement with our XRD analysis. Pure La_2O_3 crystallizes at temperatures above 640 °C [28,29]. However, all these catalysts were synthesized at room temperature and the supporting oxides were pre-calcined at 450 °C. Clearly, the incorporation of La into CeO_2 did not result in high crystallization temperatures, even for very high La contents.

BET surface area and pore volume of select samples as determined via BET and BJH analysis of nitrogen sorption, respectively, are shown in Table 2. One can see that addition of La initially results in an increase in total surface area, up to a maximum value of ≈120 m^2/g for $La_{0.25}Ce_{0.75}O_{1.875}$, and a decreasing surface area for higher La contents. The pore volume follows similar trends, although the maximum is not as pronounced and appears slightly shifted towards higher La loadings.

Upon deposition of Au, the trends in surface area and pore volume remain unchanged, although absolute values for both decrease slightly by about 10%. This suggests that the Au nanoparticles are well dispersed on the supports and may result in some pore blockage.

3.3. Effect of La content on reducibility

In order to evaluate the effect of the La doping on the reducibility of the pure and mixed La/Ce-oxides, H_2-TPR experiments were performed on samples with and without Au loading. Fig. 6 shows the result for select samples over a range of La loadings.

The TPR curve for pure CeO_2 shows two reduction peaks at 429 °C and 787 °C, respectively. The low-temperature reduction peak can be attributed to the reduction of surface oxygen and the high-temperature reduction peak to the reduction of bulk ceria and the formation of lower oxides of Ce. The incorporation of La facilitates the bulk reduction, as indicated by the shift in the high-temperature peak from 787 °C for CeO_2 to below 650 °C for all mixed $La_xCe_{1-x}O_{2-0.5x}$. This can be explained by an increase in oxygen mobility due to the formation of defects in the oxygen sublattice by introduction of the lower-valent La. (It should be noted that the pronounced peaks for $La_{0.75}Ce_{0.25}O_{1.625}$ and La_2O_3 in the 500–700 °C temperature range are not due to sample reduction, but to decomposition of carbonates. La_2O_3 is well known to form surface hydroxy-carbonates, $La_2(OH)_4(CO_3)$, when exposed to air

Table 2
Physical properties of $La_xCe_{1-x}O_{2-0.5x}$ catalysts with and without Au.

Sample	Surface area (m^2/g)		Pore volume (cm^3/g)		Particle size (nm)
	Support	With Au	Support	With Au	Support
CeO_2	103.7	87.3	0.10	0.10	7.6
$La_{0.1}Ce_{0.9}O_{1.95}$	112.7	99.3	0.15	0.14	n.d.
$La_{0.25}Ce_{0.75}O_{1.875}$	120.4	116.5	0.18	0.16	5.8
$La_{0.5}Ce_{0.5}O_{1.75}$	115.7	82.1	0.18	0.14	5.1
$La_{0.75}Ce_{0.25}O_{1.625}$	72.7	53.4	0.20	0.16	4.6
La_2O_3	52.9	24.0	0.18	0.11	8.5

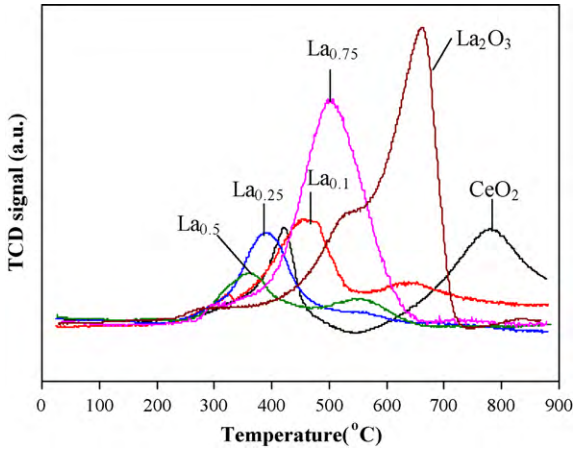

Fig. 6. H_2-TPR of select $La_xCe_{1-x}O_{2-0.5x}$ samples with varying La content.

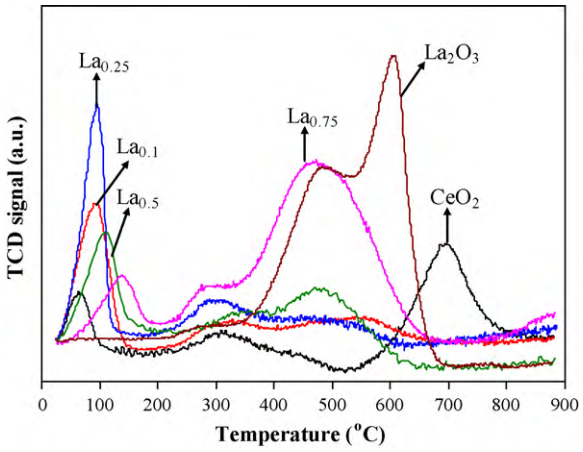

Fig. 8. H_2-TPR of select $Au/La_xCe_{1-x}O_{2-0.5x}$ samples.

[30], which then decompose to $La_2O_2CO_3$ at ~500 °C, and further to La_2O_3 between 600 °C and 800 °C, in agreement with the observed peaks [30,31].)

For the water gas shift reaction, however, the low-temperature surface reduction is the relevant reaction, since it occurs in the temperature range of interest for WGS (T < 450 °C). Fig. 7 shows that this surface reduction peak shifts continuously towards lower temperature with increasing La doping (black triangles). Only $La_{0.1}Ce_{0.9}O_{1.95}$ shows a slightly increased peak temperature, although the onset reduction temperature (208 °C) is again lower than that of pure CeO_2 (281 °C).

Beyond the reduction temperature, which indicates the reducibility of the oxides, the peak area in TPR is proportional to the H_2 consumption and hence measures the number of reducible sites, i.e. oxygen availability. Fig. 7 shows the peak areas of the low-temperature peaks for all samples vs. La content. One can see that the peak area initially increases significantly with La doping between 10% and 25%, and then drops steeply with further La addition. These results hence indicate that, while addition of large amounts of La increases the reducibility of CeO_2, i.e. makes the oxygen available at lower temperature, it also strongly reduces the number of reducible oxygen sites in the sample [26].

The reducibility of these samples is strongly affected by Au deposition, as shown in Fig. 8. The reduction temperatures for the surface oxide are lowered in comparison to the Au-free samples in Fig. 6. For samples with less than 50% La, the surface reduction peak is shifted about 100 °C towards lower temperature, while it is shifted only 30–40 °C for those with higher La content. The reason for this might be that samples with lower La content have more surface oxygen, which is much more directly affected by the deposition of Au on the surface. Such a promotion of the surface reducibility in the presence of a noble metal has been reported before [11], and has been ascribed to a weakening of the surface oxygen bond in the presence of the noble metal, thereby improving the reducibility of the catalyst [32].

The high-temperature bulk reduction process, on the other hand, is controlled by the slow diffusion of the oxygen vacancies created at the oxide surface into the bulk. Therefore, Au deposition has only a very minor effect on the bulk reduction temperature.

Most significantly, however, a new reduction peak appears in the TPR profile of $Au/La_xCe_{1-x}O_{2-0.5x}$ at much lower temperature than the surface reduction temperature. This peak is generally explained by the reduction of oxygen species on Au nanoparticles [32–36] or the hydrogen spill-over from the metal to the support [37–39]. Since the surface reduction peak area is strongly reduced upon Au deposition (cf. Figs. 6 and 8), this indicates that much of the surface oxygen has already been reduced at the new low-temperature peak. It seems therefore more likely that hydrogen adsorption and dissociation on the Au nanoparticles, followed by H spill-over onto the oxide support, is responsible for the observed peak.

Fig. 9 shows that this new low-temperature reduction peak shifts continuously to higher temperature with increasing La content, while the peak area shows again the same trend as observed in the absence of Au, i.e. it first increases to a maximum at ~25% La and then decreases strongly with further increase in La content.

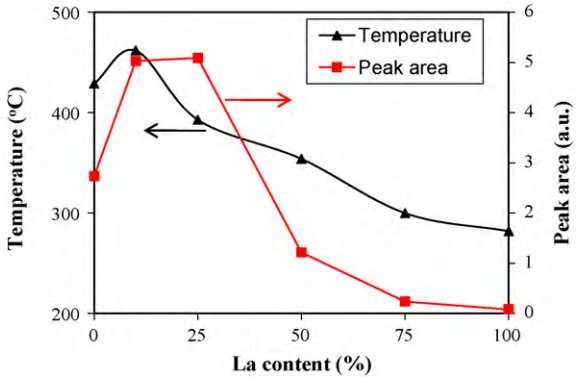

Fig. 7. Temperature and peak area of surface reduction peak select $La_xCe_{1-x}O_{2-0.5x}$ samples vs. La content.

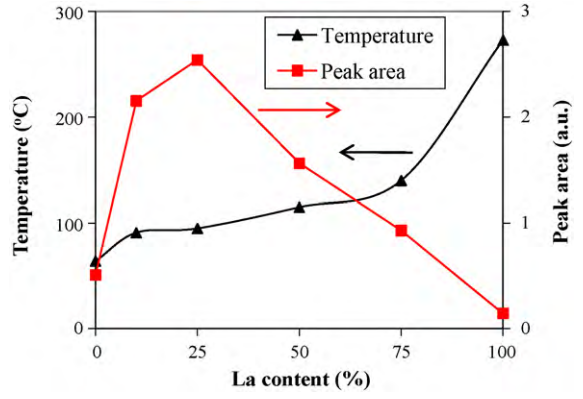

Fig. 9. Temperature and peak area of reduction peak lower than 200 °C vs. La content of select $Au/La_xCe_{1-x}O_{2-0.5x}$ samples.

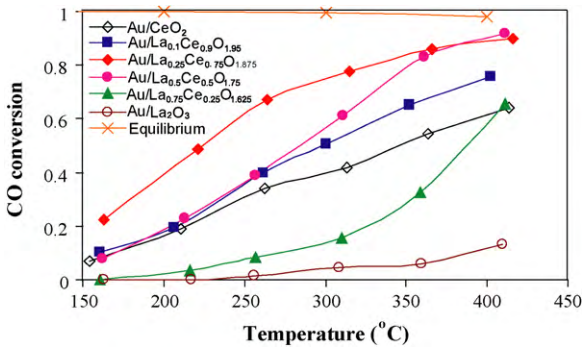

Fig. 10. Catalytic activity of $Au/La_xCe_{1-x}O_{2-0.5x}$ catalysts in WGS. CO conversion is shown as function of reaction temperature.

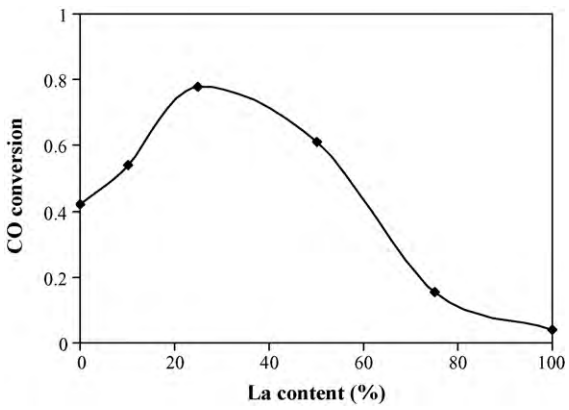

Fig. 11. Catalytic activity of $Au/La_xCe_{1-x}O_{2-0.5x}$ catalysts in WGS at 310 °C.

Overall, we hence observe an improvement in the reducibility of the oxides upon La addition which can be ascribed to the formation of oxygen vacancies. These vacancies are known to play a key role in many oxidation reactions catalyzed by metal oxide catalysts via Mars-van Krevelen and related mechanisms [19,40–42]. The oxygen vacancies are formed upon La^{3+} insertion into the CeO_2 lattice due to different valences of the metals, and favor the mobility of lattice oxygen, resulting in lower reduction temperatures. However, on the other hand, more La^{3+} also causes the decrease of available lattice oxygen since oxygen is much more strongly bound to La than to Ce, resulting in a maximum in oxygen availability at moderate La loadings.

Addition of Au nanoparticles results in the increased surface reducibility due to La addition being superseded by a new low-temperature reduction facilitated by the presence of Au. However, the total availability of low-temperature reducible oxygen is still controlled by the amount of La addition, and one can hence expect that a moderate amount of La doping should result in the most active WGS catalyst.

3.4. Effect of La content on WGS activity

The effect of La doping on catalytic activity of $Au/La_xCe_{1-x}O_{2-0.5x}$ in WGS was tested in fixed-bed reactor studies (see Section 2.2 for experimental details). Fig. 10 summarizes the results for selected $Au/La_xCe_{1-x}O_{2-0.5x}$ samples, ranging from pure CeO_2 to pure La_2O_3 supports, in terms of CO conversion as function of temperature.

As expected, Au/CeO_2 shows much higher activity than Au/La_2O_3, which can be ascribed to the reducibility of the supporting oxides. As shown above, CeO_2 is reducible in this temperature range, but La_2O_3 is non-reducible, and the importance of the reducibility of the support for WGS is well-established [35]. For the mixed oxides, the activity of the catalysts initially increases with La doping up to ~25% La, and then decreases again with further La addition. This trend can be more clearly seen in Fig. 11, where CO conversion is shown as a function of La content for one fixed reaction temperature. Comparing the curve in Fig. 11 to the reducibility trend in Fig. 7, one can clearly see that both closely follow the same trends with La content, suggesting that it is indeed the reducibility of the oxide that has a determining effect on the activity of the catalysts.

It should be mentioned that the oxidation state of Au is known to have a significant impact on the activity of Au in WGS [12]. From the present study it cannot be excluded that addition of La affects the catalytic activity by altering the oxidation state of Au at working conditions, although the direct comparison between the $Au/La_xCe_{1-x}O_{2-0.5x}$ samples and the Au-free oxides suggests that the reducibility of the oxide is in fact the dominating factor.

4. Summary

The present study aimed to elucidate the impact of La addition on structure and reducibility of CeO_2, and on the reactivity of Au-based La/Ce-mixed oxides in WGS. By utilizing a well-controlled microemulsion-templated approach, we were able to prepare highly homogeneous mixed La/Ce-oxides over the entire range of La:Ce-ratios. Both the structure and reducibility of the oxides could be tailored by adjusting the La content. The reducibility of the Au-free oxides is improved through La addition, while the availability of reducible oxygen sites displays a maximum at 25% La and then drops for higher loadings. Both effects can be traced back to the formation of oxygen vacancies, which improve oxygen mobility, and the formation of more strongly bound oxygen upon La addition.

Deposition of Au onto these oxides gives rise to an additional, low-temperature reduction peak, presumably due to hydrogen spill-over from the noble metal onto the oxide support. Preparation of $Au/La_xCe_{1-x}O_{2-0.5x}$ catalysts via deposition–precipitation furthermore showed strong dependence on pH, with optimum pH values being a function of La content. The WGS activity of $Au/La_xCe_{1-x}O_{2-0.5x}$ catalysts synthesized at optimum pH values demonstrates that appropriate La addition can result in strong increases in reactivity. Most significantly, the WGS activity of $Au/La_xCe_{1-x}O_{2-0.5x}$ could be closely correlated with the reducibility of the oxide supports.

Overall, the study demonstrates that carefully controlled synthesis of nanostructured catalysts with uniform, tailored composition allows for fine control of reactive properties of these materials, and might ultimately open the way towards a more rational design of catalysts.

Acknowledgements

This work was supported by the National Energy Technology Laboratory's on-going research under the RDS Contract DE-AC26-04NT41817, by the Department of Energy – Basic Energy Science through Grant DE-FG02-05ER46233, and by the National Science Foundation through Grant CTS-0553365. G.V. gratefully acknowledges a CNG faculty fellowship of the University of Pittsburgh's Swanson School of Engineering.

References

[1] W. Vielstich, A. Lamm, H.A. Gasteiger, Handbook of Fuel Cells: Fundamentals, Technology, and Applications, Wiley, Chichester, England, New York, 2003.
[2] C. Song, Catal. Today 77 (2002) 17–49.
[3] P. Koci, M. Schejbal, J. Trdlicka, T. Gregor, M. Kubicek, M. Marek, Catal. Today 119 (2007) 64–72.

[4] P. Koci, F. Plat, J. Stepanek, S. Bartova, M. Marek, M. Kubicek, V. Schmeisser, D. Chatterjee, M. Weibel, Catal. Today 147 (2009) S257–S264.
[5] P. Mannila, T. Salmi, H. Haario, M. Luoma, M. Harkonen, J. Sohlo, Appl. Catal. B 7 (1996) 179–198.
[6] B. Whittington, C. Jiang, D. Trimm, Catal. Today 26 (1995) 41–45.
[7] P. Panagiotopoulou, D. Kondarides, Catal. Today 112 (2006) 49–52.
[8] S. Arrii, F. Morfin, A. Renouprez, J. Rousset, J. Am. Chem. Soc. 126 (2004) 1199–1205.
[9] K. Azzam, I. Babich, K. Seshan, L. Lefferts, J. Catal. 251 (2007) 163–171.
[10] W. Deng, C. Carpenter, N. Yi, M. Flytzani-Stephanopoulos, Top. Catal. 44 (2007) 199–208.
[11] Q. Fu, A. Weber, M. Flytzani-Stephanopoulos, Catal. Lett. 77 (2001) 87–95.
[12] Q. Fu, H. Saltsburg, M. Flytzani-Stephanopoulos, Science 301 (2003) 935–938.
[13] J. Rodriguez, S. Ma, P. Liu, J. Hrbek, J. Evans, M. Perez, Science 318 (2007) 1757–1760.
[14] J. Rodriguez, P. Liu, J. Hrbek, J. Evans, M. Perez, Angew. Chem. Int. Ed. 46 (2007) 1329–1332.
[15] T. Bunluesin, R. Gorte, G. Graham, Appl. Catal. B 15 (1998) 107–114.
[16] S. Ricote, G. Jacobs, M. Milling, Y. Ji, P. Patterson, B. Davis, Appl. Catal. A 303 (2006) 35–47.
[17] A. Kozlov, D. Kim, A. Yezerets, P. Andersen, H. Kung, M. Kung, J. Catal. 209 (2002) 417–426.
[18] A. Bueno-Lopez, K. Krishna, M. Makkee, J. Moulijn, J. Catal. 230 (2005) 237–248.
[19] C. Bozo, N. Guilhaume, J. Herrmann, J. Catal. 203 (2001) 393–406.
[20] M. Kirchhoff, U. Specht, G. Veser, Nanotechnology 16 (2005) S401–S408.
[21] F. Moreau, G. Bond, A. Taylor, J. Catal. 231 (2005) 105–114.
[22] C. Guzmán, G. Del Angel, R. Gómez, F. Galindo, R. Zanella, G. Torres, C. Angeles-Chavez, J.L.G. Fierro, J. Nano Res. 5 (2009) 13–23.
[23] A. Wolf, F. Schuth, Appl. Catal. A 226 (2002) 1–13.
[24] M. Kosmulski, Chemical Properties of Material Surfaces, Marcel Dekker, New York, 2001.
[25] J. Lewis, J. Am. Ceram. Soc. 83 (2000) 2341–2359.
[26] S. Liang, E. Broitman, Y. Wang, A. Cao, V. Götz, Chem. Mater., submitted for publication.
[27] R. Fuentes, L. Acuna, M. Zimic, D. Lamas, J. Sacanell, A. Leyva, R. Baker, Chem. Mater. 20 (2008) 7356–7363.
[28] X. Wang, M. Wang, H. Song, B. Ding, Mater. Lett. 60 (2006) 2261–2265.
[29] G.A.H. Mekhemer, B.A.A. Balboul, Colloid Surf. A 181 (2001) 19–29.
[30] S. Bernal, F.J. Botana, R. García, J.M. Rodríguez-Izquierdo, React. Solids 4 (1987) 23–40.
[31] B. Klingenberg, M.A. Vannice, Chem. Mater. 8 (1996) 2755–2768.
[32] S. Scire, S. Minico, C. Crisafulli, C. Satriano, A. Pistone, Appl. Catal. B 40 (2003) 43–49.
[33] Q. Fu, S. Kudriavtseva, H. Saltsburg, M. Flytzani-Stephanopoulos, Chem. Eng. J. 93 (2003) 41–53.
[34] V. Idakiev, T. Tabakova, A. Naydenov, Z. Yuan, B. Su, Appl. Catal. B 63 (2006) 178–186.
[35] A. Sandoval, A. Gomez-Cortes, R. Zanella, G. Diaz, J. Saniger, J. Mol. Catal. A: Chem. 278 (2007) 200–208.
[36] D. Andreeva, V. Idakiev, T. Tabakova, L. Ilieva, P. Falaras, A. Bourlinos, A. Travlos, Catal. Today 72 (2002) 51–57.
[37] F. Boccuzzi, A. Chiorino, M. Manzoli, D. Andreeva, T. Tabakova, J. Catal. 188 (1999) 176–185.
[38] S. Collins, J. Cies, E. del Rio, M. Lopez-Haro, S. Trasobares, J. Calvino, J. Pintado, S. Bernal, J. Phys. Chem. C 111 (2007) 14371–14379.
[39] G. Jacobs, S. Ricote, P. Patterson, U. Graham, A. Dozier, S. Khalid, E. Rhodus, B. Davis, Appl. Catal. A 292 (2005) 229–243.
[40] D. Mullins, S. Overbury, J. Catal. 188 (1999) 340–345.
[41] Z. Pu, X. Liu, A. Jia, Y. Xie, J. Lu, M. Luo, J. Phys. Chem. C 112 (2008) 15045–15051.
[42] L. Liotta, M. Ousmane, G. Di Carlo, G. Pantaleo, G. Deganello, G. Marci, L. Retailleau, A. Giroir-Fendler, Appl. Catal. A 347 (2008) 81–88.